

Monolayer Iron Carbide Films on Au(111) as a Fischer–Tropsch Model Catalyst

Gilb  re J. A. Mannie,*†‡ Lutz Lammich,† Yong-Wang Li,§ J. W. (Hans) Niemantsverdriet,‡ and Jeppe V. Lauritsen†

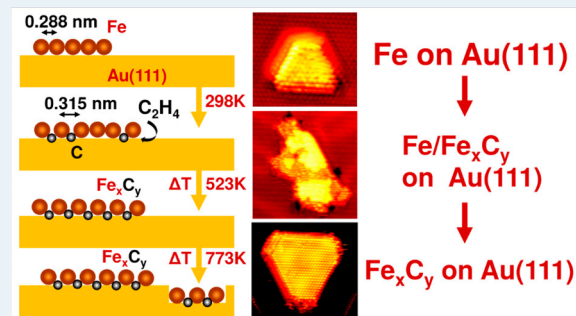
†Interdisciplinary Nanoscience Center (iNANO) and Department of Physics and Astronomy, Aarhus University, Gustav Wieds Vej 14, DK-8000 Aarhus C, Denmark

‡Syngaschem BV, Eindhoven University of Technology, P.O. Box 513, NL-5600 MB Eindhoven, The Netherlands

§Synfuels China Company Ltd., Huairou district, Beijing 101400, China

Supporting Information

ABSTRACT: Using scanning tunneling microscopy (STM), we characterize the atomic-scale details of ultrathin films of iron carbide (Fe_xC_y) on Au(111) synthesized as a potential model system for the active iron carbide phase in iron Fischer–Tropsch synthesis (FTS) catalysts. The experiments show that room-temperature exposure of Fe islands gas to C_2H_4 deposited on the clean Au(111) surface results in partly converted $\text{Fe}/\text{Fe}_x\text{C}_y$ islands. Multistep flash-heating treatment of the partly converted $\text{Fe}/\text{Fe}_x\text{C}_y$ islands at 523 and 773 K results in pure highly crystalline Fe_xC_y islands with in-plane nearest-neighbor distances of 0.315 ± 0.005 nm. On the basis of the atom-resolved STM data, we propose that C_2H_4 dissociates at Fe island edges, after which the carbon diffuses inward into the interstitial region between the Fe and the Au substrate to form an Fe_xC_y surface that may be a good starting point for the investigation of iron carbide surfaces present under FTS conditions.



KEYWORDS: scanning tunneling microscopy, iron carbide, Fischer–Tropsch synthesis, model catalyst, thin films

1. INTRODUCTION

Iron-based Fischer–Tropsch synthesis (Fe-FTS) is one of the most investigated catalytic processes in the world because of its ability to convert any form of hydrocarbons like coal, natural gas, or biomass into wax, diesel, gasoline, and chemicals.^{1,2} Although they have been investigated for almost a century, fundamental surface reactions involved in this process are still not fully understood, and several proposals for reaction pathways are available in the literature.^{3–5} For the iron-catalyzed FTS, iron carbide is seen as a key compound in these surface reactions, and several studies have been performed on the identification of these carbides.^{6–10} To study fundamental surface chemistry in detail, surface science experiments like, e.g., CO absorption on single-crystal surfaces of the most common iron carbides in Fe-FTS (ϵ' - $\text{Fe}_{2,2}\text{C}$, ϵ - Fe_3C , θ - Fe_3C , and χ - Fe_5C_2) would be a good start in understanding the actual elementary reactions during Fe-FTS. A Mars–Van Krevelen (MvK)-type reaction in which lattice C in the Fe-carbide surface is retrieved during the FTS reaction has been proposed, but the atomic-scale surface structure and the exact nature and location of carbon on the surface are not known.^{3,4} Unfortunately, iron carbide single crystals are not commercially available because of the brittle nature of the material and must therefore be synthesized before the absorption experiments. Formation of iron carbide structures on, e.g., an Fe(100)

surface is possible, but these surfaces are hard to clean and difficult to maintain in top condition because of high reactivity toward oxygen, sulfur, and carbon impurities. A more elegant method for gaining access to iron carbide model catalysts that are also flat enough to apply scanning tunneling microscopy (STM) is by synthesizing thin films on top of a noble metal substrate like Au(111). This method has been very successful for many catalytic systems like MoS_2 , V_2O_5 , and TiO_2 ^{11,12} and was also used by Weiss and Ranke to study the surface chemistry and catalytic activity of iron oxide thin films.¹³

In this work, we describe a method of synthesizing iron carbide thin films starting from submonolayer iron islands deposited on Au(111), followed by carburization in ethylene. We used atom-resolved STM to follow the carburization process. The incorporation of carbon into the iron matrix appears to be facile, and we characterize the structure of Fe_xC_y as an iron monolayer on top of a gold substrate with interstitial carbon atoms. Although synthesized Fe_xC_y structures do not fully mimic the carbide structures present in Fe-FTS synthesis, the Fe_xC_y islands can act as an attractive first surface science model system for studying the incorporation of carbon into

Received: June 25, 2014

Revised: August 16, 2014

Published: August 19, 2014



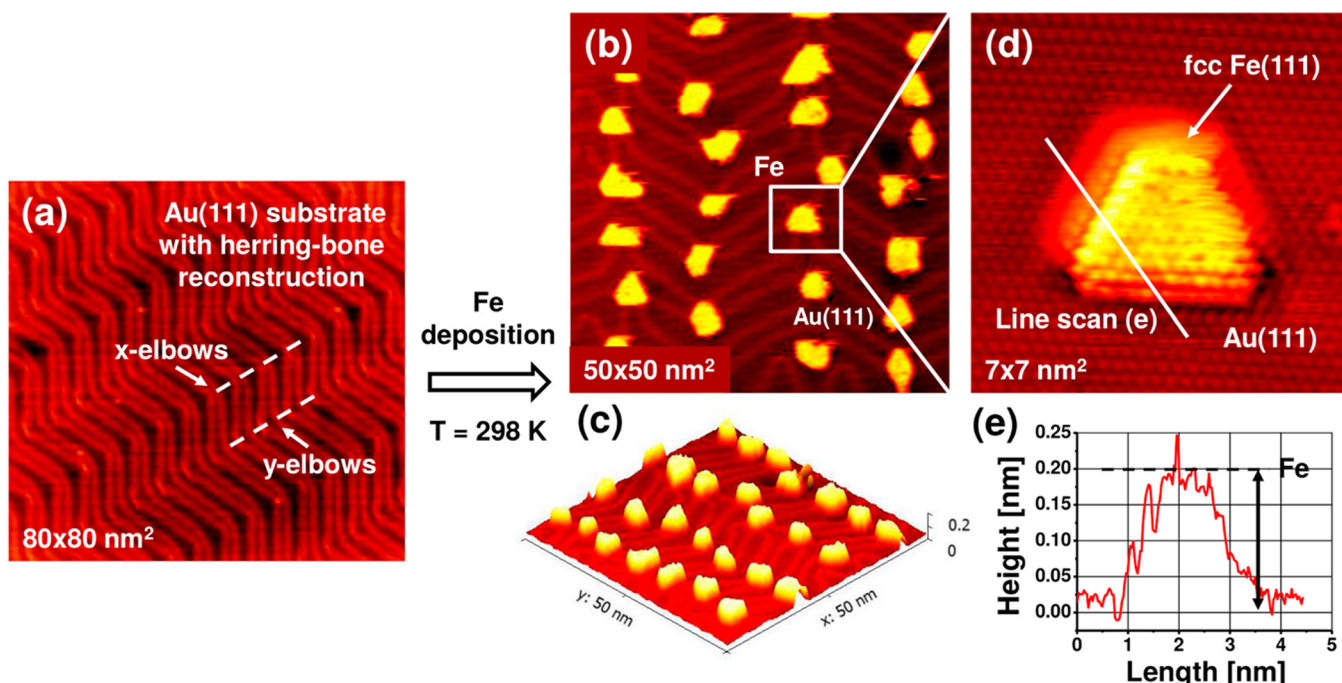


Figure 1. Scanning tunneling microscopy (STM) images of the deposition of Fe on Au(111). (a) STM image ($V_t = -4.0$ mV; $I_t = -1.6$ nA) of a clean Au(111) substrate with the characteristic “herringbone” pattern. (b and c) Three-dimensional STM images ($V_t = 1.8$ mV; $I_t = 1.6$ nA) of the monolayer Fe islands on Au(111) with a ~0.4 ML Fe coverage. (d) Atomically resolved STM image ($V_t = -0.9$ mV; $I_t = -4.1$ nA) of the top facet of an Fe island. (e) Line scan on the Fe island displayed in panel d.

iron islands and the behavior of iron carbide during exposure to synthesis gas. Using this method, we can investigate the proposed MvK-type reaction mechanism in great detail to improve our understanding of the chemistry behind Fe-based FTS.

2. EXPERIMENTAL SECTION

A Au(111) crystal was cleaned by cycles of Ar⁺ sputtering [$p(\text{Ar}) = 1 \times 10^{-5}$ mbar at 1.5 keV for 15 min] at room temperature and annealed in ultrahigh vacuum (UHV) at 850 K. Before every deposition experiment, the Au(111) crystal was annealed in oxygen [$p(\text{O}_2) = 1 \times 10^{-6}$ mbar for 1 h] to remove iron impurities because of the possible alloying of Fe into the Au crystal.¹⁴ The cleanliness of the crystal surface was examined from atomically resolved STM images. Submonolayer quantities of Fe (Goodfellow, 99.99%) were deposited on the Au(111) crystal at room temperature using an electron-beam evaporator (Oxford Applied Research, EGCO4). Deposition rates were ~0.2 ML min⁻¹, and coverages were estimated on the basis of the visible Fe in Fe/Au(111) samples using STM. Subsequently, the Fe monolayers were exposed to C₂H₄ (Air Liquide, 99.95%) for 15 min at room temperature using a directional doser, which yields an estimated local pressure of ~10⁻⁴ mbar, corresponding to 90000 L.

After the dosing experiment, we applied flash-heating to increase both the reactivity and the mobility for the system. The best results were obtained using a flash-heat step to 523 K (2 K s⁻¹, 1 min dwell time), followed by cooling to room temperature and a subsequent second flash-heat step to 773 K (2 K s⁻¹, 1 min dwell time) with again a subsequent cooling to room temperature.

STM experiments were performed in a UHV chamber with a base pressure of 2×10^{-10} mbar using a home-built Aarhus STM instrument¹⁵ with a mechanically cut Pt/Ir tip in

constant-current mode at room temperature. Images were taken using a relatively high current (~0.5 nA) and low bias voltage (~1.5 mV), and only one type of imaging mode was observed. STM movies were recorded using the same STM setup while dosing C₂H₄ at pressures between 5×10^{-8} and 5×10^{-7} mbar without a doser. Ethylene exposures during this movie are displayed in Langmuirs (1 Langmuir = 10^{-6} Torr s⁻¹).

3. RESULTS

3.1. Deposition of Fe on Au(111) Substrates. First we focus on the deposition of submonolayer iron on Au(111). Au belongs to the class of face centered cubic (fcc) metals and has a nearest-neighbor distance of 0.288 nm in the (111) plane. However, clean Au(111) surfaces do not terminate with a perfect (111) face but reconstruct into the characteristic “herringbone” pattern with a $(22 \times \sqrt{3})$ unit cell due to a contraction of the lattice distance in the topmost layer.^{12,16} Figure 1a shows a STM image of a clean Au(111) surface indicating both x- and y-elbows, which form walls between fcc and hcp stacking domains and can act as preferred nucleation sites for epitaxial growth of Fe, as demonstrated by several authors.^{17–20} During our initial deposition experiments, we have varied the deposition conditions until we found the conditions to deposit Fe with ~0.2 ML min⁻¹, which are ideal for the desired coverages around 0.4 ML. After deposition, several STM images were taken, as summarized in Figure 1b–d. Figure 1b shows epitaxially grown Fe islands (Fe coverage ~0.4 ML), separated from each other due to the expected nucleation on the x- and y-elbows of the herringbone reconstruction and Figure 1c shows a 3D representation of the same area as in Figure 1b. Figure 1d displays an atomically resolved STM image of one of the Fe islands on Au(111), showing a pseudomorphic fcc Fe(111) ordering, with a lattice distance of

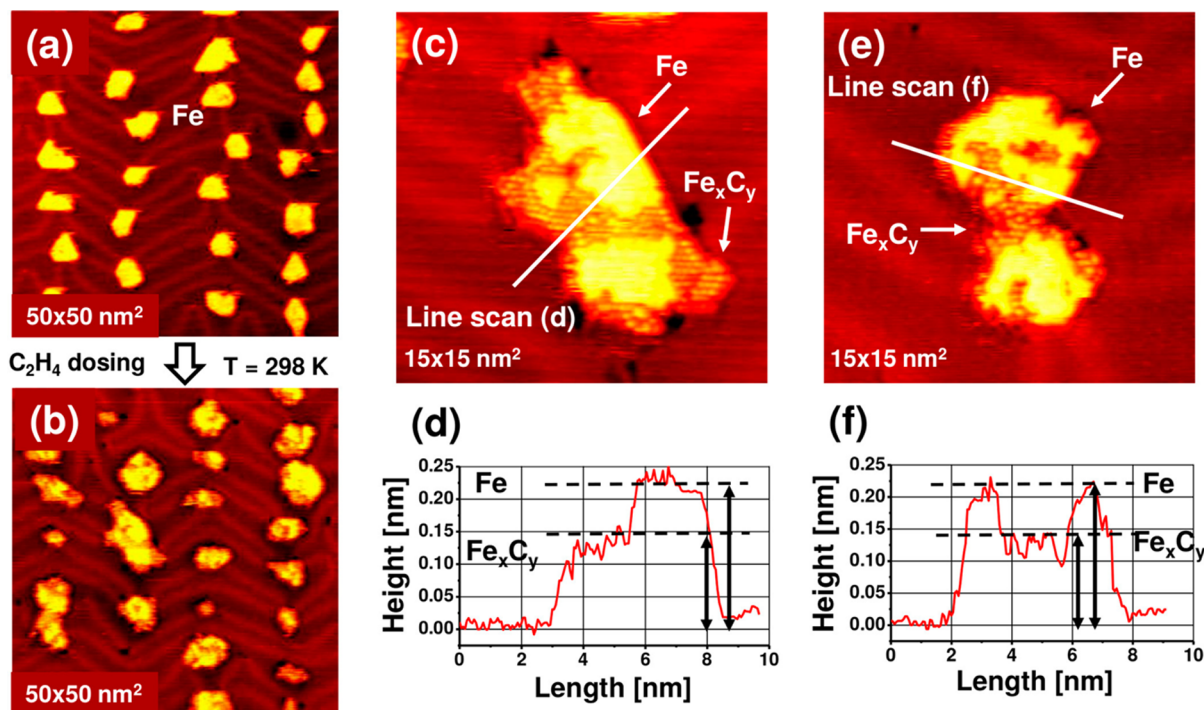


Figure 2. STM images illustrating the conversion of Fe into Fe_xC_y . (a) STM image ($V_t = 1.8 \text{ mV}$; $I_t = 1.6 \text{ nA}$) of small Fe monolayer islands on Au(111). (b) STM image ($V_t = -1.5 \text{ mV}$; $I_t = -0.5 \text{ nA}$) of Fe/ Fe_xC_y islands on Au(111). (c and e) STM images ($V_t = -1.5 \text{ mV}$; $I_t = -0.5 \text{ nA}$) of individual Fe/ Fe_xC_y islands on Au(111). (d and f) Line scans of the images in panels c and e, respectively.

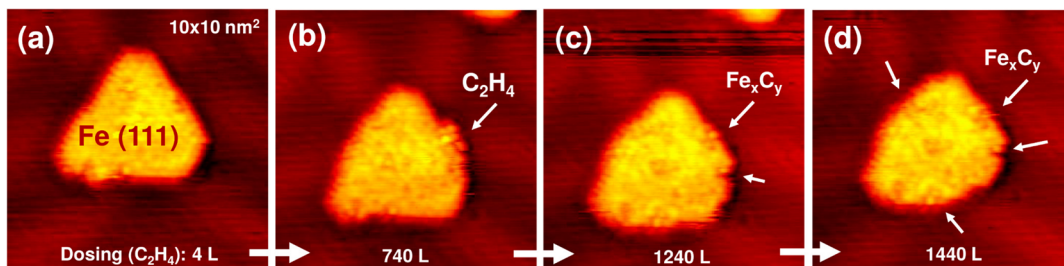


Figure 3. Stills from a STM movie ($V_t = -0.9 \text{ mV}$; $I_t = -0.6 \text{ nA}$) showing C_2H_4 dosing of pure Fe islands. (a) Fe island with a fcc Fe(111) morphology. (b) C_2H_4 adsorption on the edges of the Fe island. (c and d) Reaction of C_2H_4 with Fe resulting in small Fe_xC_y domains incorporated into the Fe island. Exposures of C_2H_4 given in Langmuirs are indicated.

$0.28 \pm 0.02 \text{ nm}$ and heights around $0.22 \pm 0.02 \text{ nm}$ (Figure 1e). The starting point for our synthesis of Fe_xC_y is therefore best characterized as monolayer Fe islands aligned with the Fe(111) facet in parallel with the Au(111) surface.

3.2. Conversion of Fe into Fe_xC_y . After observing the STM images of submonolayer Fe islands in Figure 1, we continue with the conversion of these into Fe_xC_y . Starting with pure Fe islands (Figure 2a), we exposed samples to ethylene (C_2H_4) at room temperature. Surprisingly, the reaction is facile enough at this temperature to result in partly converted Fe/ Fe_xC_y islands as seen in the STM images in panels b, c, and e of Figure 2. The images show a clear difference between the metallic Fe domains (bright area) in the center of the islands and the Fe_xC_y domains (less bright, atomically resolved) on the edges of the islands. The similar coverage and island size of the samples before (Figure 2a) and after the C_2H_4 dosing (Figure 2b) suggest a reaction and direct conversion of the Fe phase into the Fe_xC_y phase without having an exchange of Fe between the islands. This effect is also observed in panels c and e of Figure 2, and we tentatively explain this “Fe to Fe_xC_y domains”

conversion” as a process in which ethylene dissociates on the Fe edges and carbon moves into the Fe monolayer and forms Fe_xC_y domains. The islands in this state consist of several separate crystalline domains, where the Fe_xC_y domain exposes a hexagonal lattice with a nearest-neighbor distance of $0.315 \pm 0.005 \text{ nm}$, i.e., a lattice expansion resulting from the incorporation of C (Figure 2c). Line scans of the Fe/ Fe_xC_y islands (Figure 2d,f) indicate apparent STM heights of $0.22 \pm 0.02 \text{ nm}$ for the Fe phase and $0.15 \pm 0.02 \text{ nm}$ for the Fe_xC_y phase. It is important to note that STM contrast reflects a convolution of electronic and geometric structure that is furthermore dependent on the bias voltage applied. Thus, the measured apparent height cannot be directly translated into geometric height but can in this case be used as a method to distinguish metallic and Fe_xC_y domains.²¹

To follow the conversion in detail, we recorded STM movies of individual Fe islands during C_2H_4 dosing at room temperature. Figure 3 shows stills from such a movie, which can be found in the Supporting Information. Starting with a freshly deposited Fe island with (111) morphology (Figure 3a),

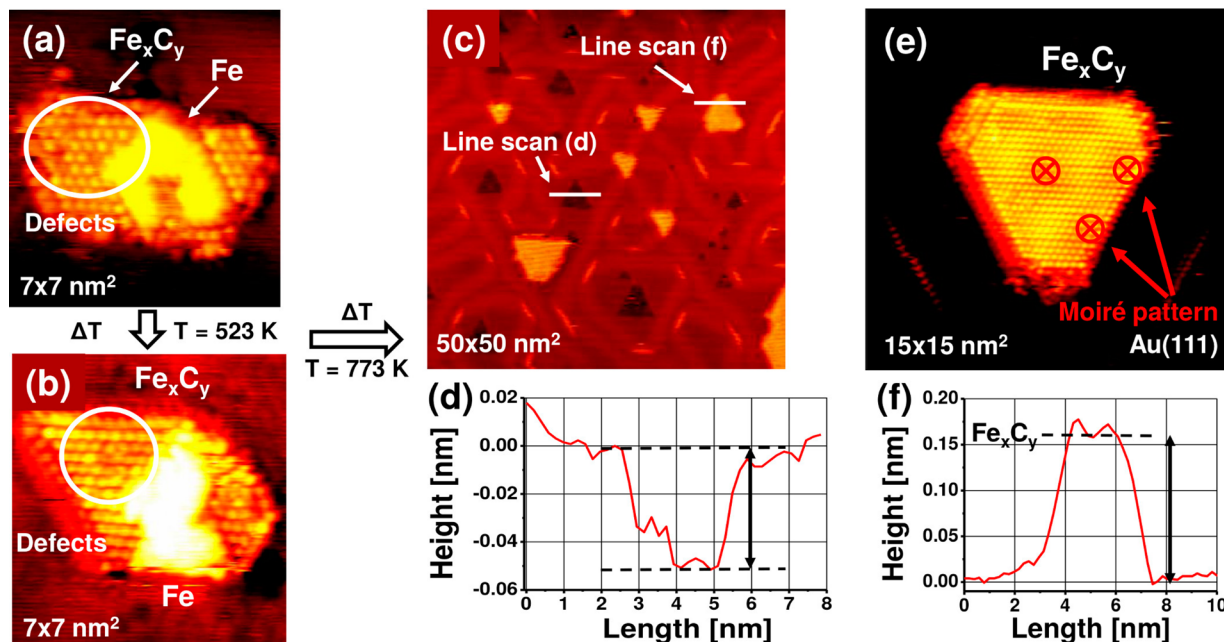


Figure 4. Atomically resolved STM images of the restructuring of Fe_xC_y islands. (a) STM image ($V_t = -1.5$ mV; $I_t = -0.5$ nA) of an $\text{Fe}/\text{Fe}_x\text{C}_y$ island on $\text{Au}(111)$ after C_2H_4 exposure at 298 K. (b) STM image ($V_t = -0.6$ mV; $I_t = -0.5$ nA) after flash-heating at 523 K. (c) STM image ($V_t = -1.5$ mV; $I_t = -1.0$ nA) after flash-heating at 773 K. (d) Line scan of the image in panel c. (e) STM image ($V_t = -2.1$ mV; $I_t = -0.9$ nA) after flash-heating at 773 K. (f) Line scan of the image in panel c.

we found dosing of C_2H_4 resulted in a highly preferred activity on the edges on the Fe islands with no visible adsorption on top of the island (Figure 3b). Most likely, C_2H_4 decomposes into C and H_2 on these edges, followed by incorporation of carbon into the iron matrix, transforming the Fe domains into small Fe_xC_y domains from the edge and inward (Figure 3c). Because of this conversion process, the shape of the Fe island is changed, starting with a triangular-shaped iron island in Figure 3a to an almost roundly shaped island in Figure 3d. The overall level of conversion during the STM movie is low compared with those of the islands shown in Figure 2, as expected on the basis of the difference in C_2H_4 exposure (STM movie, 1440 L; Figure 2, samples made using a directional gas doser at 90000 L).

3.3. Restructuring of Carburized Iron Islands. To obtain highly crystalline Fe_xC_y islands, flash-heating was applied to the $\text{Fe}/\text{Fe}_x\text{C}_y$ samples to increase both mobility within and reactivity of the Fe islands. Figure 4 shows atomically resolved STM images of the different steps in this procedure, with partly converted $\text{Fe}/\text{Fe}_x\text{C}_y$ islands containing point defects caused by incomplete carburization in panels a and b of Figure 4 and fully converted Fe_xC_y islands in panels c and e of Figure 4. During the flash-heating steps, samples were first flashed to the intermediate temperature of 523 K and subsequently cooled to room temperature. During this first step, an increase in crystallinity can be observed (Figure 4b), but with metallic iron domains still present. Afterward, a second flash-heating step to 773 K and cooling step to room temperature was conducted, resulting in highly ordered structures of pure Fe_xC_y domains (Figure 4c,e), with nearest-neighbor distances of 0.315 ± 0.005 nm and heights of 0.15 ± 0.02 nm (Figure 4f). Also visible on the top facet of the Fe_xC_y islands in Figure 4e is a large-scale moiré pattern with a nearest-neighbor distance of 3.3 ± 0.2 nm and a small corrugation. Moiré patterns are superstructures that arise due to the incommensurate growth of an overlayer on a

substrate, and they are frequently observed in heteroepitaxial thin film growth. The observed 3.3 nm moiré periodicity is in a simple one-dimensional (nonrotated) model an exact match to the case of an expanded Fe lattice (0.315 ± 0.005 nm) on the $\text{Au}(111)$ lattice (0.288 ± 0.005 nm). It is interesting to note that next to the Fe_xC_y islands, a second type of structure with a depression of 0.05 ± 0.01 nm (Figure 4e) is present, which we believe to be monolayer islands of Fe_xC_y incorporated into the top layer of the $\text{Au}(111)$ crystal because of alloying. The presence of graphene layers resulting from the ethylene decomposition (lattice constant of 0.232 nm²²) can be ruled out because the nearest-neighbor distance of 0.315 nm in Figure 4e is significantly larger.

4. DISCUSSION

We summarize the observations leading to synthesis of thin iron carbide films on a $\text{Au}(111)$ surface with the help of Figure 5.

The deposition of iron on $\text{Au}(111)$ yields monolayer pseudomorphic islands with $\text{Fe}(111)$ structure because of the preferential nucleation on the x - and y -elbows of the “herringbone reconstructed” $\text{Au}(111)$ (Figure 5a). Island heights are 0.22 ± 0.02 nm, and in-plane nearest-neighbor distances are 0.28 ± 0.02 nm, which are in full agreement with literature values for $\text{Fe}/\text{Au}(111)$.^{17–20} On this basis, we conclude that monolayer Fe islands have an $\text{Fe}(111)$ structure in our samples.

Subsequent C_2H_4 exposure of the islands at room temperature yields partly converted islands in which the $\text{Fe}(111)$ -like island is partly replaced by atomically resolved domains, which we assign to Fe_xC_y as seen in STM images (Figure 2) and a STM movie (Figure 3). The conversion happens at room temperature, which is consistent with the observation that C_2H_4 decomposition can take place at temperatures below 250 K on $\text{Fe}(111)$.^{23,24} Our STM movie indicates that C_2H_4 decom-

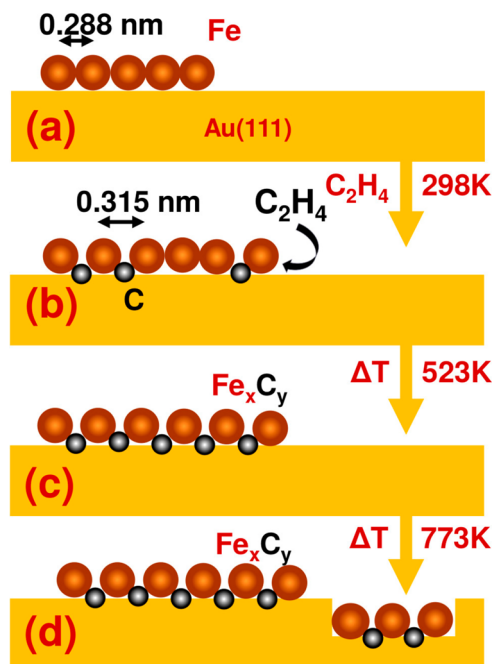


Figure 5. Schematic representation of the steps in the formation of Fe_xC_y islands. (a) Monolayer Fe islands on Au(111). (b) C₂H₄ exposure of the Fe islands leads to decomposition of C₂H₄ on Fe island edges with subsequent interstitial C between Fe and Au(111). (c) Flash-heating to 523 K accelerates the carburization process and increases the crystallinity. (d) Flash-heating to 773 K leads to incorporation of Fe_xC_y into the top layer of Au(111).

position takes place on iron island edges, which in this case is similar to preferential C₂H₄ decomposition and carbon growth on step edges of Ni(111)^{25,26} (Figure 5b). Conversion is not yet complete as metallic Fe domains are observed in the center of the islands. Fe_xC_y domains with in-plane nearest-neighbor distances of 0.315 ± 0.005 nm suggest an expanded Fe lattice (0.288 ± 0.01 nm),¹⁸ which is attributed to interstitial carbon incorporation. From the STM data alone, the location of the carbon cannot be deduced directly, but we tentatively propose a geometry with either carbon sandwiched between the Fe and Au(111) in an sp³-like configuration as illustrated in Figure 5b or alternatively in-plane sp²-like carbon between the iron atoms. Comparison of the nearest-neighbor distance with those of other known iron carbides present during Fe-FTS did not result in identification of the synthesized carbide.^{1,10,27}

Subsequent flash-heating of the partly converted Fe/Fe_xC_y islands increases the reactivity and mobility of the reactants, which results in the disappearance of defects and the further conversion of the iron domains (Figure 5c). The first effect can be explained by the higher mobility of the interstitial carbon atoms at elevated temperatures, resulting in a complete filling of interstitial carbon sites, whereas the second effect is probably due to alloying of remnant iron with the Au(111) crystal,¹⁴ resulting in separation of the Fe and Fe_xC_y by incorporation of Fe into the bulk of Au(111). The observed depressions in the Au(111) surface may tentatively be assigned to incorporation of monolayer Fe_xC_y islands into the top layer of the Au(111) surface (as presented in Figure 5d). The depression depth of 0.05 ± 0.01 nm (Figure 4d) is equal to the difference between the Au(111) step (0.288 nm) and an Fe_xC_y monolayer (0.22 nm). This phenomenon of layer incorporation has been proposed previously by Padovani et al.²⁸ and Fonin et al.²⁹

The obtained pure iron carbide thin films consist of iron layers with interstitial carbon atoms that can be used to develop well-defined Fe-FTS model catalysts. Advantages are the *in situ* synthesis and the possibility of studying the iron carbide with STM to obtain atom-resolved information, but a possible drawback could be the relatively thin iron carbide layers that are possibly thinner than the Fe_xC_y skin layer formed under Fe-FTS conditions.

5. CONCLUSIONS

In conclusion, we have synthesized ultrathin iron carbide films on Au(111) that are promising model catalysts suitable for surface science studies on iron Fischer–Tropsch catalysis. Straightforward deposition on monolayer Fe films on a Au(111) substrate, followed by a room-temperature conversion with C₂H₄, resulted in mixed Fe/Fe_xC_y islands, which we believe are the result of C₂H₄ decomposition on the edges of the islands followed by incorporation of carbon into the iron lattice. Subsequent flash-heating steps reduced the amount of point defects and eventually transformed the Fe/Fe_xC_y islands into pure highly crystalline Fe_xC_y islands. In future work, we plan to combine further STM studies of the synthesized Fe_xC_y islands with DFT calculations of structure and energetics and in particular the MvK mechanism proposed by Niemantsverdriet and co-workers.^{3,4} These experiments are expected to provide a more detailed understanding of the Fe-FTS model catalyst system for surface science studies.

■ ASSOCIATED CONTENT

Supporting Information

One AVI video file (8.7 MB) of the STM movie. This material is available free of charge via the Internet at <http://pubs.acs.org>.

■ AUTHOR INFORMATION

Corresponding Author

*E-mail: gilbere@syngaschem.com.

Notes

The authors declare no competing financial interest.

■ ACKNOWLEDGMENTS

We thank Dr. Alexander S. Walton for fruitful scientific discussions and support during the experimental work. This work was financed by Syngaschem BV and Synfuels China Company Ltd.

■ REFERENCES

- (1) de Smit, E.; Weckhuysen, B. M. *Chem. Soc. Rev.* **2008**, *13*, 2758–2781.
- (2) van de Loosdrecht, J.; Botes, F. G.; Ciobica, I. M.; Ferreira, A.; Gibson, P.; Moodley, D. J.; Saib, A. M.; Visagie, J. L.; Weststrate, C. J.; Niemantsverdriet, J. W. Fischer–Tropsch synthesis: Catalysts and Chemistry. In *Comprehensive Inorganic Chemistry II*; Reedijk, J., Poeppelmeier, K., Eds.; Elsevier: Oxford, U.K., 2013; Vol. 7, pp S25–S57.
- (3) Gracia, J. M.; Prinsloo, F. F.; Niemantsverdriet, J. W. *Catal. Lett.* **2009**, *133*, 257–261.
- (4) Ozbek, M. O.; Niemantsverdriet, J. W. *J. Catal.* **2014**, *317*, 158–166.
- (5) Govender, A.; Curulla-Ferré, D.; Pérez-Jigato, M.; Niemantsverdriet, J. W. *Molecules* **2013**, *18*, 3806–3824.
- (6) Raupp, G. B.; Delgass, W. N. *J. Catal.* **1979**, *58*, 348–360.
- (7) Niemantsverdriet, J. W.; van der Kraan, A. M.; van Dijk, W. L.; van der Baan, H. S. *J. Phys. Chem.* **1980**, *84*, 3363–3370.

- (8) Niemantsverdriet, J. W.; van der Kraan, A. M. *J. Catal.* **1981**, *72*, 385–388.
- (9) Le Caër, G.; Dubois, J. M.; Pijolat, M.; Perrichon, V.; Bussière, P. *J. Phys. Chem.* **1982**, *86*, 4799–4808.
- (10) de Smit, E.; Cinquini, F.; Beale, A. M.; Safanova, O. V.; van Beek, W.; Sautet, P.; Weckhuysen, B. M. *J. Am. Chem. Soc.* **2010**, *132*, 14928–14941.
- (11) Lauritsen, J. V.; Kibsgaard, J.; Helvig, S.; Topsøe, H.; Clausen, B. S.; Lægsgaard, E.; Besenbacher, F. *Nat. Nanotechnol.* **2007**, *2*, 53–58.
- (12) Gong, J. *Chem. Rev.* **2012**, *112*, 2987–3054.
- (13) Weiss, W.; Ranke, W. *Prog. Surf. Sci.* **2002**, *70*, 1–151.
- (14) Christiansen, A.; Ruban, A. V.; Stoltze, P.; Jacobsen, K. W.; Skriver, H. L.; Nørskov, J. K.; Besenbacher, F. *Phys. Rev. B* **1997**, *56*, 5822–5834.
- (15) Lægsgaard, E.; Besenbacher, F.; Mortensen, K.; Stensgaard, I. J. *Microsc.* **1988**, *152*, 663–669.
- (16) Barth, J. V.; Brune, H.; Ertl, G.; Behm, R. J. *Phys. Rev. B* **1990**, *42*, 9307–9318.
- (17) Voigtländer, B.; Meyer, G.; Amer, N. M. *Surf. Sci.* **1991**, *255*, L529–L535.
- (18) Stroscio, J. A.; Pierce, D. T.; Dragoset, R. A.; First, P. N. *J. Vac. Sci. Technol., A* **1992**, *10*, 1981–1985.
- (19) Khan, N. A.; Matranga, C. *Surf. Sci.* **2008**, *602*, 932–942.
- (20) Donati, F.; Mairov, A.; Casari, C. S.; Passoni, M.; Li Bassi, A. *Surf. Sci.* **2012**, *606*, 702–710.
- (21) Tersoff, J.; Hamann, D. R. *Phys. Rev. B* **1985**, *31*, 805–813.
- (22) Vinogradov, N. A.; Zakharov, A. A.; Kocevski, V.; Rusz, J.; Simonov, K. A.; Eriksson, O.; Mikkelsen, A.; Lundgren, E.; Vinogradov, A. S.; Mårtensson, N.; Preobrajenski, A. B. *Phys. Rev. Lett.* **2012**, *109*, 026101.
- (23) Seip, U.; Tsai, M.-C.; Küppers, J.; Ertl, G. *Surf. Sci.* **1984**, *147*, 65–88.
- (24) Somorjai, G. A. *J. Phys. Chem.* **1990**, *94*, 1013–1023.
- (25) Vang, R. T.; Honkkala, K.; Dahl, S.; Vestergaard, E. K.; Schnadt, J.; Lægsgaard, E.; Clausen, B. S.; Nørskov, J. K.; Besenbacher, F. *Surf. Sci.* **2006**, *600*, 66–77.
- (26) Saadi, S.; Abild-Pedersen, F.; Helvig, S.; Sehested, J.; Hinnemann, B.; Appel, C. C.; Nørskov, J. K. *J. Phys. Chem. C* **2010**, *114*, 15432–15439.
- (27) Du Plessis, H. E. Crystal structures of the iron carbides. Ph.D. Thesis, University of Johannesburg, Johannesburg, South Africa, 2008.
- (28) Padovani, S.; Scheurer, F.; Bucher, J. P. *Europhys. Lett.* **1999**, *45*, 327–333.
- (29) Fonin, M.; Dedkov, Y. S.; Rüdiger, U.; Güntherodt, G. *Surf. Sci.* **2003**, *529*, L275–L280.